Available online at www.sciencedirect.com
SCIENCE DIRECT®
Journal of Power Sources 132 (2004) 219–224
JOURNAL OF POWER SOURCES
www.elsevier.com/locate/jpowsour

Short communication

Properties of $Li[Cr_xLi_{(1-x)/3}Mn_{2(1-x)/3}]O_2$ ($0.1 \leq x \leq 0.2$) material prepared by quenching

Xianglan Wu*, Kwang Sun Ryu, Young-Sik Hong, Yong Joon Park, Soon Ho Chang

Basic Research Laboratory, Electronics and Telecommunications Research Institute, 161 Gajeong-dong, Yuseong-gu, Daejeon 305-350, South Korea

Received 29 August 2003; accepted 21 December 2003

Abstract

$Li[Cr_xLi_{(1/3-x/3)}Mn_{(2/3-2x/3)}]O_2$ materials with $x = 0.1$, 0.15, and 0.2 are prepared by a solution method. The materials are calcined at 900 °C for 12 h in air, and then quenched to room temperature. The quenching procedure results in material with improved capacity and rate capability. In fact, layered $Li_{1.27}Cr_{0.2}Mn_{0.53}O_2$ not only shows a good cycle performance, but also exhibits an excellent discharge capacity of around 260 mA h g^{-1}. Cyclic voltammetry and a.c. impedance spectroscopy are also employed to characterize the reversibility and reactions of lithium insertion and extraction in $Li[Cr_xLi_{(1/3-x/3)}Mn_{(2/3-2x/3)}]O_2$ electrodes.

Keywords: Layered material; Quenching; Lithium chromium manganese oxide; Intercalation; Lithium battery; High capacity

1. Introduction

Lithium chromium manganese oxides with various compositions have been studied by several groups [1–11]. Among these, $Li[Cr_xLi_{(1/3-x/3)}Mn_{(2/3-2x/3)}]O_2$ with an α-$NaFeO_2$ structure is the most attractive material. It was reported that $Li[Li_{0.2}Cr_{0.4}Mn_{0.4}]O_2$ ($x = 0.4$) delivers a reversible capacity of 170 mA h g^{-1} with good capacity retention at a current density of 7.5 mA g^{-1} [6]. Similarly, $Li[Cr_xLi_{(1/3-x/3)}Mn_{(2/3-2x/3)}]O_2$ ($x = 1/4$ and 1/3) was found to deliver around 200 mA h g^{-1} with excellent cycling retention at a current density of 5 mA g^{-1} [11]. In both cases, the heat-treatment was carried out under an inert atmosphere. By contrast, $Li_3CrMnO_{4+\delta}$ ($x = 0.4$) prepared by treating oxide slurry with 4 M LiOH solution in a tube furnace under flowing air was shown to give a large reversible capacity of 220 mA h g^{-1} at a current density of 3.6 mA g^{-1}. Unfortunately, the capacity dropped to 160 mA h g^{-1} when the current density was raised to 14.4 mA g^{-1} and 140 mA h g^{-1} when the current was 28.8 mA g^{-1} [5]. These results are consistent with a previous investigation that concluded that oxide powders must either be quenched or cooled in a reducing gas atmosphere to retain the high-temperature phase. Cooling in a reducing gas atmosphere may result, however, in displacive phase transformation [12].

Recently, it was reported that manganese-rich $Li[Ni_xLi_{(1/3-2x/3)}Mn_{(2/3-x/3)}]O_2$ ($x \leq 1/3$) prepared by quenching takes an α-$NaFeO_2$ structure and show a large reversible capacity of 225 mA h g^{-1} with excellent cycleability [13]. It was also reported that quenched $Li[Ni_xLi_{(1/3-2x/3)}Mn_{(2/3-x/3)}]O_2$ gives higher capacity and rate capability than that of a slowly cooled counterpart. On the other hand, it was reported that discharge capacity tends to increase with increase in the Cr:Mn ratio when the heat-treatment is performed under an inert atmosphere [6]. Based on this, we have synthesized a manganese-rich compound, viz., $Li[Cr_xLi_{(1/3-x/3)}Mn_{(2/3-2x/3)}]O_2$ ($0.1 \leq x \leq 0.2$), with an α-$NaFeO_2$ structure by quenching in anticipation that it will give large reversible capacity and improved rate capability.

2. Experimental

Layered $Li[Cr_xLi_{(1/3-x/3)}Mn_{(2/3-2x/3)}]O_2$ was prepared from a mixture of manganese acetate, chromium acetate and lithium hydroxide using a solution method. A solution of LiOH was added, with stirring, to a pre-dissolved solution of manganese acetate and chromium acetate. This resulted in a homogeneous precipitation solution. The mixed precipitation solution was heated on a hot plate until it became a viscous inorganic polymer. It was then coated on a titanium foil and heated on a hot plate to give porous powders. The powders were fired at 700 °C for 3 h and then calcined

* Corresponding author. Tel.: +82-42-860-6891; fax: +82-42-860-6836.
E-mail address: wxlpostech@yahoo.com (X. Wu).

0378-7753/$ – see front matter © 2004 Elsevier B.V. All rights reserved.
doi:10.1016/j.jpowsour.2003.12.030

at 900 °C for 12 h in air. This was followed by a quenching procedure to room temperature. Powder X-ray diffraction (XRD) measurements were conducted by means of a MAC science MXP3A-HF diffractometer using Cu Kα radiation. Scanning electron microscopy (SEM) was performed with a Philips SEM 535M instrument that had an accelerating voltage of 10 kV. The cycling performance of the positive-electrode (cathode) materials was evaluated using pouch-type cells that used a negative electrode of lithium metal foil and a separator. Cathodes were prepared by mixing $Li[Cr_xLi_{(1/3-x/3)}Mn_{(2/3-2x/3)}]O_2$ powders, super P black (MMM Carbon Co.), and poly(vinylidene)fluoride (PVDF) binder in a ratio of 85:7.5:7.5 by weight. The mixture was formed into a slurry in *N*-methyl-2-pyrrolidone (NMP) solution and cast as a film on aluminum foil by the doctor blade method. The cast was dried at 130 °C for 12 h in vacuum and then pressed into an appropriate thickness in a roll press. The electrolyte was 1 M $LiPF_6$ dissolved in 1:1 ethylene carbonate (EC) and dimethyl carbonate (DMC). Cells were cycled galvanostatically over the potential range of 2.0–4.9 V using a Maccor Battery Tester System.

Cyclic voltammetry (CV) and a.c. impedance spectroscopy were also carried out with pouch-type cells. The voltammograms were obtained using a scan rate of 0.05 mV s^{-1} over a potential range of 2.0–4.9 V versus a Li/Li^+ reference electrode. Impedance experiments were carried out in the frequency range from 0.1 Hz to 100 kHz with an a.c. voltage signal of ±5 mV. The CV experiments were performed by means of a computer controlled Biologic Macpile multichannel instrument, while impedance spectroscopy was conducted with a Solartron impedance analyzer (SI 1260) coupled to a battery test unit.

3. Results and discussion

X-ray diffraction patterns for $Li[Li_{(1/3-x/3)}Cr_xMn_{(2/3-2x/3)}]O_2$ ($x = 0.1$, 0.15, and 0.2) are shown in Fig. 1. All of the peaks correspond to a hexagonal α-$NaFeO_2$ structure, except the superlattice ordering peaks between 20° and 30°. The latter peaks, which result from the short-range ordering of Li, Cr and Mn atoms in the transition metal layers, appear less pronounced with increase in chromium content [11]. The unit cell parameters for these compounds are presented in Table 1. The contraction along the *a*-axis with increase in chromium content may be associated with a more uniform substitution of Cr in $LiMnO_2$ compounds.

Table 1
Hexagonal unit cell parameters for $Li[Li_{(1/3-x/3)}Cr_xMn_{(2/3-2x/3)}]O_2$ materials calcined at 900 °C

Composition	*a* (Å)	*c* (Å)	*c*/*a*
$Li_{1.3}Cr_{0.1}Mn_{0.6}O_2$	2.849	14.247	5.000
$Li_{1.28}Cr_{0.15}Mn_{0.57}O_2$	2.853	14.264	4.999
$Li_{1.27}Cr_{0.2}Mn_{0.53}O_2$	2.854	14.264	4.997

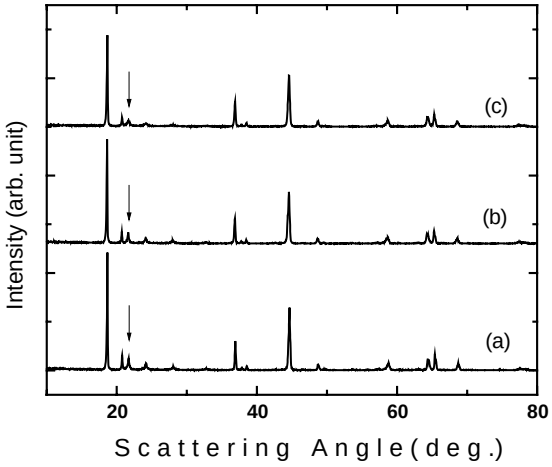

Fig. 1. Powder X-ray diffraction patterns of (a) $Li_{1.3}Cr_{0.1}Mn_{0.6}O_2$, (b) $Li_{1.28}Cr_{0.15}Mn_{0.57}O_2$ and (c) $Li_{1.27}Cr_{0.2}Mn_{0.53}O_2$. Peaks in the arrow-marked region correspond to superlattice ordering.

The morphology of $Li[Li_{(1/3-x/3)}Cr_xMn_{(2/3-2x/3)}]O_2$ ($x = 0.1$, 0.15, and 0.2) is shown in Fig. 2. The particles of these materials exhibit equiaxed hexagonal shapes with well-developed crystal faces. The average crystal size of $Li_{1.3}Cr_{0.1}Mn_{0.6}O_2$, $Li_{1.28}Cr_{0.15}Mn_{0.57}O_2$, and $Li_{1.27}Cr_{0.2}Mn_{0.53}O_2$ is 0.8, 0.5, and 0.3 μm, respectively. It is obvious that the particle size decreases with increase in chromium content. On the other hand, it has been reported [7] that manganese oxide has a considerably greater tendency for crystal growth via a solid-state reaction. Therefore, the abnormally large particles may be attributed to the Mn-rich content.

The first few charge and discharge curves for a $Li|Li_{1.27}Cr_{0.2}Mn_{0.53}O_2$ cell cycled between 2.0 and 4.9 V with a current density of 12 mA g^{-1} are given in Fig. 3. It is clear that the first charge profile is distinctly different from the subsequent ones, and the irreversible capacity loss is up to 115 mA h g^{-1}. With further cycling, both the capacity and the voltage profile are stable which indicates that the structure is stable over the entire intercalation–deintercalation range. Similar behavior was reported [14,15] for $Li[Ni_xLi_{(1/3-2x/3)}Mn_{(2/3-x/3)}]O_2$ with α-$NaFeO_2$ structure and it was ascribed to the transfer of some transition metals into the lithium layer on de-lithiation. It was further explained that these heavy cations in the Li layer inhibit the insertion of lithium into every available site due to slow diffusion. By contrast, for Li_2MnO_3 with the same structure, it was suggested that the irreversible capacity results from the reaction of Li^+ with H^+ generated by electrolyte oxidation on charge. On the subsequent discharge, electrochemical reduction within the electrolyte consumes H^+ thus drives its extraction from the electrode and its replacement by Li^+ [16]. In the present study, the irreversible capacity increases with increase in chromium content but does not change by varying the insertion rate or electrolyte content. Therefore, the dramatic loss of capacity on the initial cycle may also

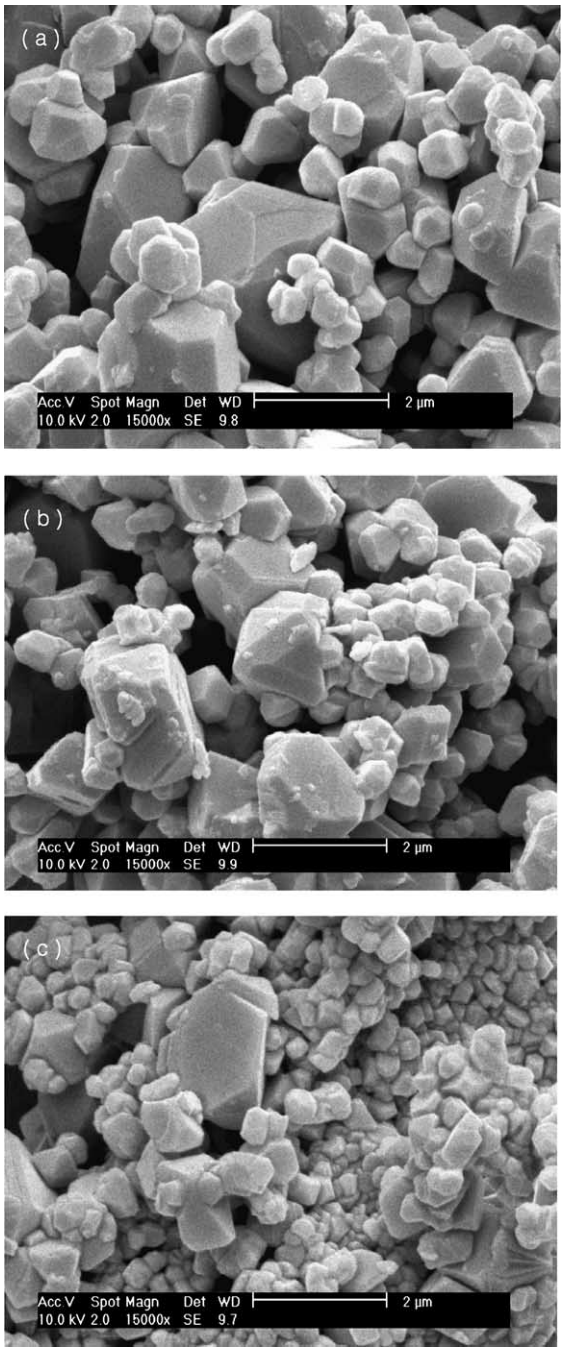

Fig. 2. Electron micrographs of (a) $Li_{1.3}Cr_{0.1}Mn_{0.6}O_2$, (b) $Li_{1.28}Cr_{0.15}Mn_{0.57}O_2$ and (c) $Li_{1.27}Cr_{0.2}Mn_{0.53}O_2$.

be associated with some structural ordering and elimination of stacking faults [13].

The first few charge and discharge curves for both $Li|Li_{1.3}Cr_{0.1}Mn_{0.6}O_2$ and $Li|Li_{1.28}Cr_{0.15}Mn_{0.57}O_2$ cells cycled between 2.0 and 4.9 V with a current density of 15 mA g^{-1} are presented in Fig. 4. The $Li|Li_{1.3}Cr_{0.1}Mn_{0.6}O_2$ cell delivered an initial capacity of 187 mA h g^{-1}, which gradually increased to 260 mA h g^{-1} within a few cycles. On the other hand, the $Li|Li_{1.28}Cr_{0.15}Mn_{0.57}O_2$ cell exhibits a slightly higher initial capacity of 225 mA h g^{-1} and the capacity is moderately increased to 248 mA h g^{-1} on cycling. The relatively low initial capacity of the material with a lower chromium content may be attributed to the initial activation of the irregularly large crystal particles, as

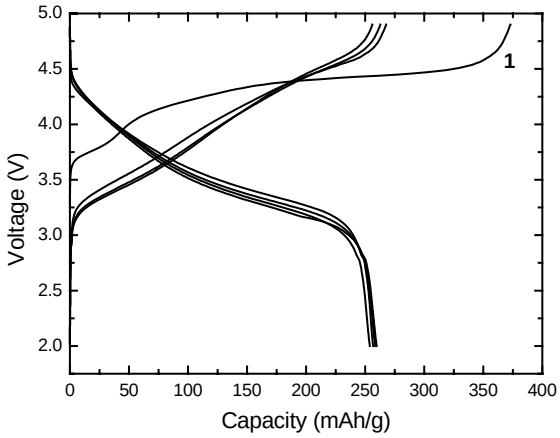

Fig. 3. Charge–discharge curves for $Li|Li_{1.27}Cr_{0.2}Mn_{0.53}O_2$ cell. Data collected with a current density of 12 mA g^{-1} in the voltage range of 2.0–4.9 V.

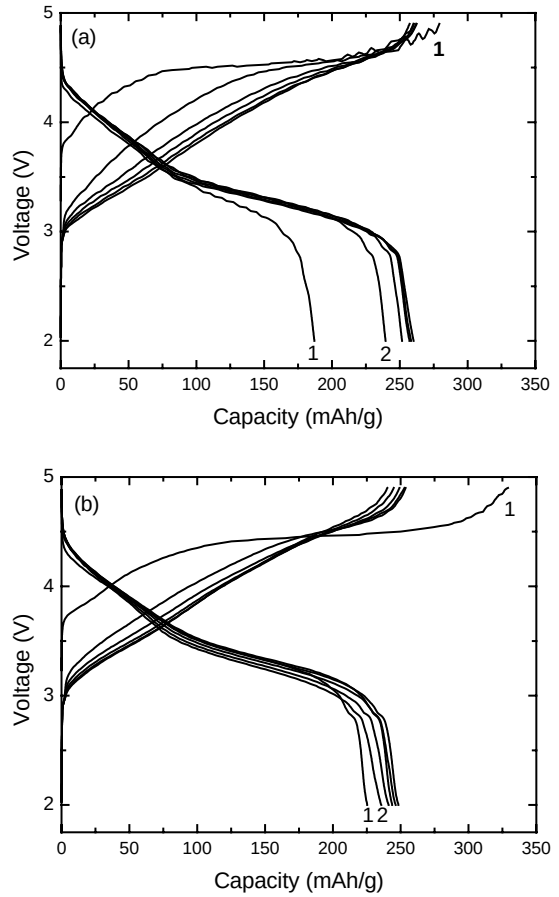

Fig. 4. Charge–discharge curves for (a) $Li|Li_{1.3}Cr_{0.1}Mn_{0.6}O_2$, and (b) $Li|Li_{1.28}Cr_{0.15}Mn_{0.57}O_2$ cells. Data were collected with a current density of 15 mA g^{-1} in the voltage range of 2.0–4.9 V.

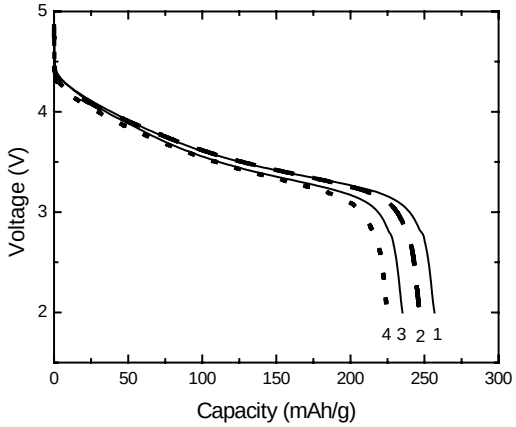

Fig. 5. Voltage vs. capacity profiles for Li|$Li_{1.27}Cr_{0.2}Mn_{0.53}O_2$ cells as a function of different discharge rates. Current densities are (1) 12 (2) 17 (3) 26 and (4) 30 mA g^{-1}.

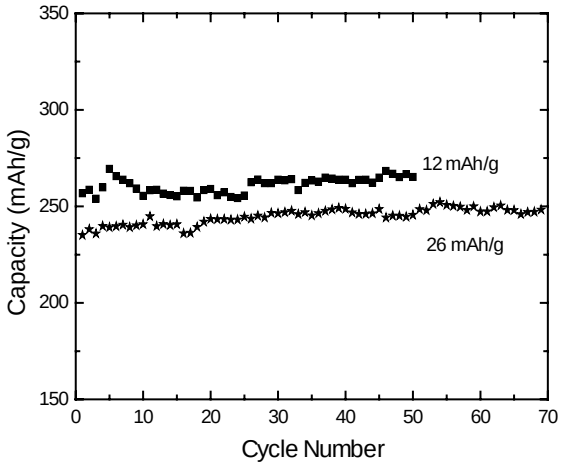

Fig. 6. Discharge capacity vs. cycle numbers for Li|$Li_{1.27}Cr_{0.2}Mn_{0.53}O_2$ cells. Data were collected with current densities of (a) 12 and (b) 26 mA g^{-1} in the voltage range of 2.0–4.9 V.

observed in SEM data (Fig. 2). In addition, the discharge curve has two slopes at a voltage of 3.5 V when $x \leq 0.1$. Although the two cells delivered a high capacity of around 250 mA h g^{-1} within a few cycles, they exhibited prominent capacity fade after 30 cycles.

The rate performance of $Li_{1.27}Cr_{0.2}Mn_{0.53}O_2$ material during the first discharge is shown in Fig. 5. The corresponding Li|$Li_{1.27}Cr_{0.2}Mn_{0.53}O_2$ cells provide 257, 247, 235 and 224 mA h g^{-1} capacity at a current density of 12, 17, 26 and 30 mA g^{-1}, respectively. It is clear that the capacity decreases slightly with increase in current density, while the average discharge voltage is stable at relatively low current densities ($\leq$17 mA g^{-1}). On the other hand, it has been reported that $Li[Li_{(1/3-x/3)}Cr_xMn_{(2/3-2x/3)}]O_2$ ($x = 1/6$ and 1/4) prepared under N_2 gas exhibited 200–230 mA h g^{-1} capacity at a current density of 5 mA g^{-1} [11]. These results reveal that quenching in air results in materials with improved capacity and rate capability. This is again consistent with the previous finding [13] that quenched $Li[Ni_xLi_{(1/3-2x/3)}Mn_{(2/3-x/3)}]O_2$ gives higher capacity than that of slowly cooled [13]. The discharge capacity versus cycle number for Li|$Li_{1.27}Cr_{0.2}Mn_{0.53}O_2$ cells cycled with the current density of 12 or 26 mA g^{-1} is shown in Fig. 6. Both cells exhibit excellent cycling retention, and the cell cycled with lower current density delivered an excellent discharge capacity of around 260 mA g^{-1} even after 50 cycles.

Cyclic voltammograms for $Li[Li_{(1/3-x/3)}Cr_xMn_{(2/3-2x/3)}]O_2$ ($x = 0.1$, 0.15, and 0.2) electrodes obtained at a scan rate of 0.05 mV s^{-1} are presented in Fig. 7. It is clear that the profile of the first cycle is quite different from the subsequent ones for all the three materials. The cathodic peak height corresponding to Li intercalation increases with cycling, while the peak positions are virtually unchanged. This indicates that the thermodynamics of Li intercalation has not changed during cycling [17]. Indeed, the observed increase in peak height may be attributed to an increase in electrical contact between the irregularly large particles of the cathode material through the initial activation processes (see Fig. 2) [7]. On the other hand, the anodic peak at 4.6 V, except that in Fig. 7(a), shows a significant decrease in intensity, while the peak around 3.8 V shifts to a more negative potential by about 0.2 V on the subsequent cycle. The negative shift reduces the separation between corresponding cathodic and anodic peaks. This indicates that the material becomes more reversible after the first charge. This observation suggests that Cr substitution also induces some structural ordering or a reduction of stacking faults during the first Li de-intercalation as in the case of $Li[Ni_xLi_{(1/3-2x/3)}Mn_{(2/3-x/3)}]O_2$ [13,18]. This is again in good agreement with the highly polarized first charge profile and the dramatic capacity loss noted in the charge and discharge curves shown in Figs. 3 and 4. By contrast, the anodic peak at 4.6 V in Fig. 7(a) exhibits a slight increase in intensity on the subsequent cycle. As mentioned above, the unusual increase in peak height may also be ascribed to an increase in electrical contact between large particles since there is still a large irreversible current between the first anodic and the corresponding cathodic peak. Besides, two, small, reversible peaks between 2.8 and 2.9 V disappear, while the cathodic peaks at 3.3 and 4.0 V tend to merge with increase in chromium content. These observations suggest that the peaks located between 3.3 and 4.6 V may be related to Cr^{3+}/Cr^{6+} and Cr^{3+}/Cr^{4+} couples, whereas the small peaks located between 2.8 and 2.9 V may be attributed to the Mn^{3+}/Mn^{4+} couple, which results from the Mn-rich phase in the presence of less chromium [18–22]. These results reinforce the previously reported conclusion, drawn from Mn K-edge XANES studies, that Mn(IV) does not show a significant change in oxidation state during the charge and the discharge processes [10].

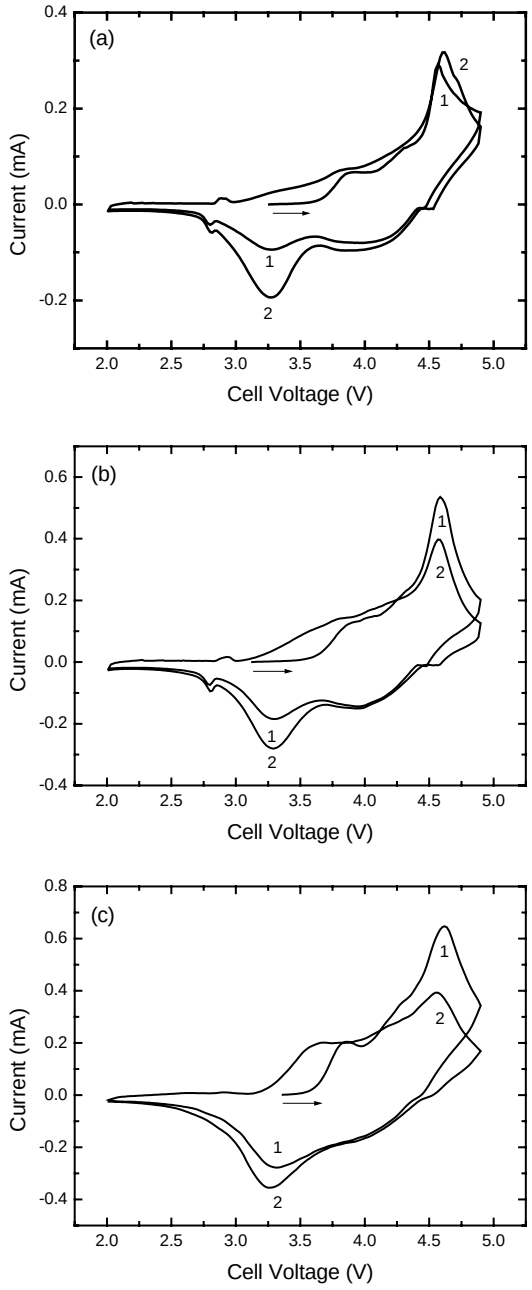

Fig. 7. Cyclic voltammograms for (a) Li|$Li_{1.3}Cr_{0.1}Mn_{0.6}O_2$, (b) Li|$Li_{1.28}Cr_{0.15}Mn_{0.57}O_2$ and (c) Li|$Li_{1.27}Cr_{0.2}Mn_{0.53}O_2$ cells at a scan rate of 0.05 mV s^{-1}.

Nyquist plots for pristine electrodes with different compositions are given in Fig. 8. Each plot consists of a depressed semicircle and a sloping line at low frequencies. The size of the semicircle scarcely changes with increase in chromium content. This demonstrates that the amount of chromium has only a minor effect on the charge-transfer resistance. On the other hand, the sloping line shows pronounced deviation from the typical Warburg impedance, which indicates that electrodes are highly resistive. Nyquist plots measured with the same electrode at 3.2 V before and after cycling are

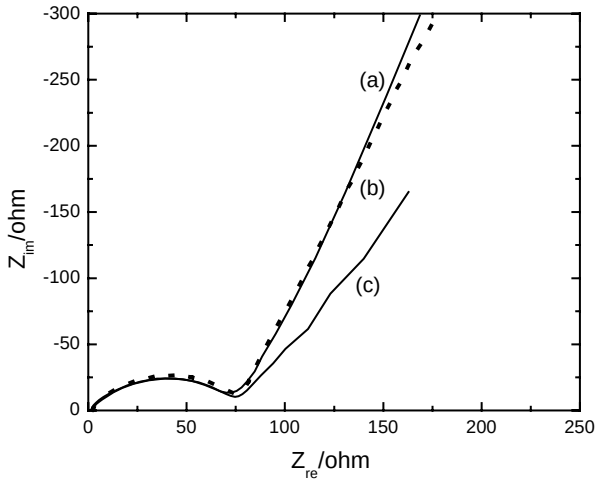

Fig. 8. Nyquist plots of (a) $Li_{1.3}Cr_{0.1}Mn_{0.6}O_2$, (b) $Li_{1.28}Cr_{0.15}Mn_{0.57}O_2$ and (c) $Li_{1.27}Cr_{0.2}Mn_{0.53}O_2$ pristine electrodes measured at 3.2 V.

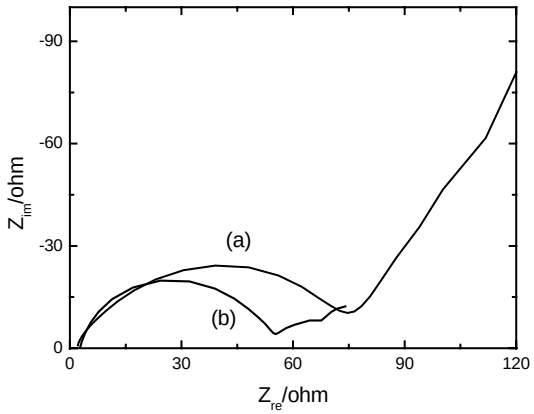

Fig. 9. Nyquist plots for $Li_{1.27}Cr_{0.2}Mn_{0.53}O_2$ electrode obtained at 3.2 V (a) pristine and (b) after cycling.

given in Fig. 9. It is clear that the charge-transfer resistance decreases upon cycling and thus speeds up the kinetics of the intercalation–de-intercalation process. This may be due to some reorganization of the active mass structure that occurs during the first charge process.

4. Conclusions

Layered $Li[Li_{(1/3-x/3)}Cr_xMn_{(2/3-2x/3)}]O_2$ ($x = 0.1$, 0.15, and 0.2) with an α-$NaFeO_2$ structure is synthesized by quenching. The quenching procedure results in materials with excellent capacity and cycleability. Indeed, a Li|$Li_{1.27}Cr_{0.2}Mn_{0.53}O_2$ cell delivered a capacity of 257 mA h g^{-1} in the first cycle and sustained around 260 mA h g^{-1} capacity even after 50 cycles. The voltammetric behavior indicates that Cr substitution induces some structural change during the first Li de-intercalation. By contrast, the thermodynamics of Li intercalation into the electrode does not change during cycling.

Acknowledgements

This work was supported by funds from the Korean Ministry of Information and Communication (MIC No. 2003-S-003).

References

[1] J. Cho, B. Park, Electrochem. Solid-State Lett. 3 (2000) 355.
[2] I.J. Davidson, R.S. McMillan, J.J. Murray, J. Power Sour. 54 (1995) 205.
[3] J. Cho, Y.J. Kim, B. Park, Solid State Ionics 138 (2001) 221.
[4] J.R. Dahn, T. Zheng, C.L. Thomas, J. Electrochem. Soc. 145 (1998) 851.
[5] C. Storey, I. Kargia, Y. Grincourt, I.J. Davidson, Y.C. Yoo, D.Y. Seung, J. Power Sour. 97–98 (2001) 541.
[6] B. Ammudsen, J. Paulsen, I. Davidson, R. Liu, C. Shen, J. Chen, L. Jang, J. Lee, J. Electrochem. Soc. 149 (2002) A431.
[7] Z.P. Guo, S. Zhong, G.X. Wang, G. Walter, H.K. Liu, S.X. Dou, J. Electrochem. Soc. 149 (2002) A792.
[8] I.J. Davidson, R.S. McMillan, H. Slegr, B. Luan, I. Kargina, J.J. Murray, I.P. Swainson, J. Power Sour. 81–82 (1999) 406.
[9] S.T. Myung, S. Komaba, N. Hirosaki, N. Kumagai, K. Arai, R. Kodama, Y. Terada, I. Nakai, Proceedings of the 11th International Meeting on Lithium Batteries, Monterey, June 23–28, 2002 (Abstract No. 90).
[10] M. Balasubramanian, J. McBreen, I.J. Davidson, P.S. Whitfiled, I. Kargina, J. Electrochem. Soc. 149 (2002) A176.
[11] Z. Lu, J.R. Dahn, Electrochem. Soc. 149 (2002) A1454.
[12] Y. Jang, W.D. Moorehead, Y. Chiang, Solid State Ionics 149 (2002) 201.
[13] Z. Lu, L.Y. Beaulieu, R.A. Donaberger, C.L. Thomas, J.R. Dahn, J. Electrochem. Soc. 149 (2002) A778.
[14] Z. Lu, J.R. Dahn, J. Electrochem. Soc. 149 (2002) A815.
[15] A. Kajiyama, K. Takada, T. Inada, M. Kouguchi, S. Kondo, M. Watanabe, J. Electrochem. Soc. 148 (2001) A981.
[16] A.D. Robertson, P.G. Bruce, Chem. Commun. 23 (2002) 2790.
[17] R. Premanand, A. Durairajan, B. Haran, R. White, B. Popov, J. Electrochem. Soc. 149 (2002) A54.
[18] K.M. Shaju, G.V. Subbarao, B.V.R. Chowdari, J. Electrochem. Soc. 150 (2003) A1.
[19] A. Kajiyama, K. Takada, K. Arihara, T. Inada, H. Sasaki, S. Kondo, M. Watanabe, J. Electrochem. Soc. 150 (2003) A157.
[20] T. Ohzuku, K. Tatsumi, N. Matoba, K. Sawal, J. Electrochem. Soc. 147 (2000) 3592.
[21] P. Arora, B.N. Popov, R.E. White, J. Electrochem. Soc. 145 (1998) 807.
[22] L. Zhang, H. Noguchi, J. Electrochem. Soc. 150 (2003) A601.